## ARTICLES

# Theoretical study of native and rare-earth defect complexes in $\beta$-$PbF_2$

Huitian Jiang, Aurora Costales,* Miguel A. Blanco,† Mu Gu,‡ and Ravindra Pandey
*Department of Physics, Michigan Technological University, Houghton, Michigan 49931*

Julian D. Gale
*Department of Chemistry, Imperial College of Science, Technology and Medicine, South Kensington, SW7 2AY London, United Kingdom*
(Received 15 November 1999; revised manuscript received 31 January 2000)

Native and rare-earth-doped point-defects in $\beta$-$PbF_2$ are studied in the framework of the pair-potential approximation coupled with the shell model description of the lattice ions. For the perfect lattice, a new set of potential parameters are obtained which reproduce structure, elastic and dielectric constants of $PbF_2$ very well. The calculated formation energies for native defects suggest that the anion Frenkel disorder is preferred over the cation Frenkel and Schottky-like disorder in $PbF_2$. The computed temperature behavior of the ionic conductivity agrees very well with the available experimental data. In the rare-earth doped $PbF_2$, a site preference of the charge-compensating fluorine interstitial appears to change from nearest to next-nearest neighbor with the increase in the rare-earth ionic radius.

### I. INTRODUCTION

There has been renewed interest in finding a candidate material for scintillating detectors to be used in the high energy physics experiments in which the particle energy exceeds GeV.[1] For this application, it is expected that such a candidate material should be of short radiation length, high light yield, short decay time, and a good radiation hardness, along with the requirement of relatively inexpensive growth process.[2,3] Conventional scintillating materials, e.g., NaI:Tl, do not satisfy these requirements due to long decay time and low density, though they produce a very high light yield. Currently, lead-based compounds, such as lead tungstate ($PbWO_4$) and lead fluoride ($PbF_2$), are the focus of research activities since they satisfy most of the criteria for being an ideal scintillating material in the high energy physics experiments.

$PbF_2$ is a fast ionic conductor at high temperatures and is also found to exhibit scintillating properties. A faint scintillation light in the orthorhombic phase of the polycrystalline $PbF_2$ was observed at room temperature, which was stimulated by a synchronous radiation x-ray source.[4] Note that $PbF_2$ crystallizes from its molten form in the $\beta$ (cubic) phase, and is known to undergo a pressure-induced phase transition at about 0.4 GPa[5,6] to the $\alpha$ (orthorhombic) phase. The experimental efforts have therefore been directed towards finding the scintillating phenomenon in the cubic phase of $PbF_2$. Recently, Shen and his co-workers have reported fast luminescent components at 277.5 and 312.4 nm, with a light yield $>6.2$ p.e./MeV, and decay time $<30$ ns in Gd-doped $\beta$-$PbF_2$ at room temperature.[7,8] The observed light output and decay is found to satisfy the requirements of a scintillation detector working both with good energy resolution and at high counting rate. While growing the single crystals of $PbF_2$, degradation in the transmissivity of the crystal has been reported due to absorption of the luminescent emission by native defects in the lattice. Furthermore, doping of rare-earth ions into $PbF_2$ raises the issue of charge compensation involving native defects in the crystalline lattice.

Although $PbF_2$ has been the subject of various experimental and theoretical investigations to understand its superionicity, its defect chemistry is rather poorly understood. Generally, its defect structure has been taken to be that of an alkaline-earth fluoride (e.g., $BaF_2$), in spite of the fact that the Pb cation is much more polarizable than any alkaline-earth cation. This difference in the polarizability is also reflected in the static dielectric constant of $PbF_2$, which is much larger than that of $CaF_2$ or $BaF_2$. Previous attempts[9,10] to study native defects of the cubic $PbF_2$ were partially successful due to a convergence failure of the shell-model calculations for the case of a fluorine vacancy. It was suggested that a quasiharmonic form of the potential representing the core-shell interaction for Pb may be needed for a successful investigation of defect properties in $PbF_2$. Following this suggestion, in this paper we have determined another set of parameters for the shell model description of the ionic interactions in the crystalline lattice and have successfully obtained the energetics of native point-defects including the fluorine vacancy in $PbF_2$. We have also calculated the activation energies for the migration of both F and Pb ions in the lattice and have considered the charge compensation mechanism in $PbF_2$ doped with rare earths. The calculated results are expected to shed light on similarities and differences between the defect chemistry of $PbF_2$ and that of alkaline-earth fluorides.

### II. METHOD

The atomistic simulation model employed here in calculations of both perfect lattices and lattices containing defects, is based on a fully ionic description of the crystalline structure.[11] In the present case, cubic $PbF_2$, whose structure

 

consists of a cubic anion sublattice with cations occupying every other (alternate) body-centered interstitial sites, can be considered as consisting of $Pb^{+2}$ and $F^-$ ions. We note here that the ionic model is often found to be a reasonable basis for interatomic potential models, as any effects of covalency can be subsumed into the parametrization for closed shell ions. The force field in this work consists of a pairwise interaction energy which is composed of a Buckingham potential, to model the short range Pauli repulsion and the leading term of the dispersion energy, plus the Coulomb interaction:

$$E_{ij}=A\exp(-r_{ij}/\rho)-Cr_{ij}^{-6}+q_i q_j/r_{ij}, \tag{1}$$

where $A$, $\rho$, and $C$ are empirically determined parameters.

Because of the conditionally convergent nature of the electrostatic interaction, an Ewald sum is used to calculate the electrostatic energy and its derivatives.[12] The partitioning between reciprocal and real space is chosen so as to minimize the total number of terms to be evaluated. Other interactions are summed directly in real space up to a cutoff of 12 Å except for the exponential repulsion, which is truncated when it becomes less than the target accuracy for the Ewald sum. The dipolar polarizability of the ions has also been included through the use of the shell model.[13] Here a massless shell of charge $Y$, on which all interatomic potentials act, is coupled by a quasiharmonic spring to a core, i.e.,

$$E_{\text{core-shell}}=\frac{1}{2}k_2 r^2+\frac{1}{24}k_4 r^4 \tag{2}$$

($k_2$ and $k_4$ are again empirical parameters), from which it is Coulombically screened, yielding an environment dependent ion polarizability. All calculations have been performed using the program GULP,[14] which optimizes the structure with respect to the asymmetric unit fractional coordinates and cell strains, using analytical symmetry-adapted first and second derivatives within a Newton-Raphson procedure starting from the exact Hessian matrix.

### A. Interatomic potentials: Host lattice

For the host lattice, formal ionic charges of $+2$ and $-1$ are assigned to Pb and F, respectively, thereby considering them as $Pb^{+2}$ and $F^-$ in $PbF_2$. The short-range interaction terms introduced by the model describe $Pb^{+2}$-$F^-$, $F^-$-$F^-$, and $Pb^{+2}$-$Pb^{+2}$ interactions. The parameters for the $F^-$-$F^-$ interaction are assumed to be transferable among a series of fluorides, and are taken from the work of Catlow *et al.*[15] They were obtained from Hartree-Fock calculations of the interaction of two fluorine ions. Model parameters that include the short-range interaction parameters for $Pb^{+2}$-$F^-$ and $Pb^{+2}$-$Pb^{+2}$ interactions, along with the shell charge and spring constants of $Pb^{+2}$ and $F^-$, are then fitted to experimentally measured lattice properties such as the structure, elastic, and dielectric constants. The relaxed fitting algorithm was used in all parameter determinations.[16] Here an optimization of the crystal structure is performed at every stage of the least squares procedure. This has the benefit that the fitted quantities become the changes in structural parameters rather than the forces calculated at the experimental structure. This is found to be a superior procedure, as minimizing the forces is not guaranteed to produce better results unless the second derivatives are also improved. Furthermore, this allows all properties included in the fit to be properly determined about the energy minimum configuration rather than at the unrelaxed experimental geometry. The final interatomic potential parameters obtained are given in Table I. As can be seen in Table II, the computed parameters reproduce the crystalline properties of $PbF_2$ very well.

TABLE I. Short-range potential and shell model parameters for cubic $PbF_2$. The charges on ions are taken to be $-1e$ and $+2e$ for F and Pb, respectively. For the definition of the $r_a$, $r_m$, and $r_b$ interpolation parameters, see Ref. 15.

(a) Shell-shell interactions

| | $A$(eV) | $\rho$(Å) | $C$(eV Å$^6$) | $r_a$ | $r_m$ | $r_b$ |
|---|---|---|---|---|---|---|
| $Pb_s$-$F_s$ | 1121.6 | 0.3309 | | | | |
| $Pb_s$-$Pb_s$ | 18 147.9 | 0.1452 | | | | |
| $F_s$-$F_s$ | 1127.7 | 0.2753 | 15.83 | 3.031 | 2.726 | 2.000 |

(b) Core-shell interactions

| | $k_1$(eV Å$^{-2}$) | $k_2$(eV Å$^{-4}$) | $Y(e)$ |
|---|---|---|---|
| $Pb_c$-$Pb_s$ | 288.0 | 40 000 | −6.65 |
| $F_c$-$F_s$ | 41.7 | 40 000 | −2.09 |

### B. Interatomic potentials: Rare earth/host lattice

In order to obtain lattice-adapted potentials, we will use *ab initio* perturbed ion ionic descriptions for the $Pb^{+2}$ and $F^-$ ions to fed the electron gas machinery, following the lines of Ref. 20. We will restrict ourselves to the so called *rigid* potentials, meaning with it that we will use a single ionic description to obtain the potential for every distance. This is in fact the most appropriate approach when dealing with defects, in which the perfect lattice structure is assumed to vary only in the vicinity of the defect center. Thus, we will consider the $\beta$-$PbF_2$ experimental geometry with ionic descriptions of $Pb^{+2}$ and $F^-$ ions. For the rare-earth ions, we have taken the *in vacuo* ionic descriptions, since the trivalent ions are not expected to change much when inserted into the lattice. We have used the multizeta Slater-type basis set of Koga *et al.*[21] for the $F^-$ anion, and the neutral atom basis sets[22] for rare earths and Pb. We have eliminated the most diffuse $p$ functions and reoptimized the external exponents in

TABLE II. Calculated bulk properties of cubic $PbF_2$. The experimental values are taken from Refs. 17–19.

| Property | Experimental | Calculated |
|---|---|---|
| Lattice constant | | |
| $a$, Å | 5.939 | 5.947 |
| Elastic constants | | |
| $C_{11}$, GPa | 88.8 | 102.0 |
| $C_{12}$, GPa | 47.2 | 35.2 |
| $C_{44}$, GPa | 24.5 | 20.9 |
| Bulk modulus | | |
| $B_0$, GPa | 61.07 | 57.48 |
| Dielectric constants | | |
| $\epsilon_0$ | 29.30 | 29.30 |
| $\epsilon_\infty$ | 3.08 | 3.09 |

TABLE III. Electron gas model short-range potential parameters for rare-earth/host lattice interactions.

| Pair | $A_{ij}$(eV) | $\rho_{ij}$(Å) | Pair | $A_{ij}$(eV) | $\rho_{ij}$(Å) |
|---|---|---|---|---|---|
| $Y^{+3}$-$F^{-}$ | 3109.8 | 0.2945 | $Y^{+3}$-$Pb^{+2}$ | 16 195.0 | 0.2399 |
| $La^{+3}$-$F^{-}$ | 3210.9 | 0.3108 | $La^{+3}$-$Pb^{+2}$ | 19 750.2 | 0.2472 |
| $Ce^{+3}$-$F^{-}$ | 3455.4 | 0.3027 | $Ce^{+3}$-$Pb^{+2}$ | 17 537.8 | 0.2560 |
| $Pr^{+3}$-$F^{-}$ | 3569.7 | 0.2990 | $Pr^{+3}$-$Pb^{+2}$ | 16 006.4 | 0.2636 |
| $Nd^{+3}$-$F^{-}$ | 3713.9 | 0.2971 | $Nd^{+3}$-$Pb^{+2}$ | 16 465.3 | 0.2619 |
| $Sm^{+3}$-$F^{-}$ | 4018.9 | 0.2932 | $Sm^{+3}$-$Pb^{+2}$ | 17 282.5 | 0.2588 |
| $Eu^{+3}$-$F^{-}$ | 4169.3 | 0.2914 | $Eu^{+3}$-$Pb^{+2}$ | 17 660.4 | 0.2573 |
| $Gd^{+3}$-$F^{-}$ | 4312.0 | 0.2898 | $Gd^{+3}$-$Pb^{+2}$ | 18 012.5 | 0.2560 |
| $Tb^{+3}$-$F^{-}$ | 4492.6 | 0.2874 | $Tb^{+3}$-$Pb^{+2}$ | 18 292.5 | 0.2549 |
| $Dy^{+3}$-$F^{-}$ | 4642.7 | 0.2857 | $Dy^{+3}$-$Pb^{+2}$ | 18 592.3 | 0.2538 |
| $Er^{+3}$-$F^{-}$ | 4949.7 | 0.2823 | $Er^{+3}$-$Pb^{+2}$ | 19 098.0 | 0.2518 |
| $Yb^{+3}$-$F^{-}$ | 5252.3 | 0.2791 | $Yb^{+3}$-$Pb^{+2}$ | 19 511.3 | 0.2502 |
| $Lu^{+3}$-$F^{-}$ | 5332.3 | 0.2786 | $Lu^{+3}$-$Pb^{+2}$ | 19 794.2 | 0.2491 |

the description of the lead cation. In the electron gas formalism, we have used the following functionals: Thomas-Fermi for kinetic energy, Lee-Lee-Parr[23] for exchange, and Clementi's new fitting[24] of the Wigner correlation functional. The resulting electron gas potentials are presented in Table III, and selected potentials are depicted in Fig. 1.

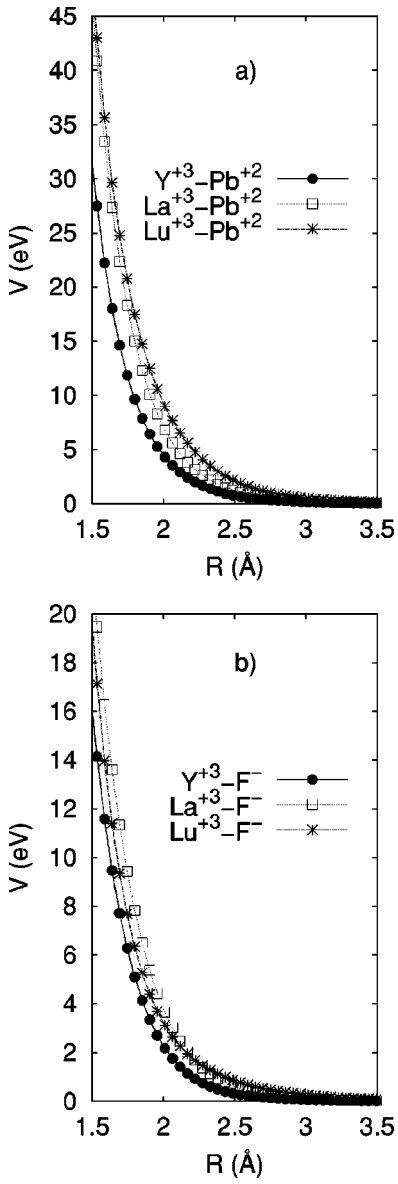


FIG. 1. Interatomic potentials of yttrium, lanthanum, and lutetium (all other rare earths fall between the last two) with the host lattice ions.

## III. RESULTS AND DISCUSSION

### A. Native defects

The formation energies of native defects have been calculated using the Mott-Littleton method.[15] Here the region of the crystal surrounding the defect is divided into three spherical regions referred to as 1, 2a and 2b. In region 1, all interactions are treated directly at an atomistic level and the ions are explicitly allowed to relax in response to the defect. Except in the case of very short-ranged defects, it is not generally possible to achieve the desired degree of convergence by increasing region 1 before running out of computer resources. Consequently, in region 2a some allowance is made for the relaxation of ions but in a way that is more approximate. In region 2a the ions are assumed to be situated in an harmonic well and they subsequently respond to the electrostatic force of the defect species accordingly. This approximation is valid for small perturbations and therefore can be used when region 1 is sufficiently large. Beyond region 2a, in region 2b, the effect of the net charge of the defect polarizing the remainder of the crystal is evaluated out to convergence by use of a partial transformation into reciprocal space, analogous to the Ewald method for the electrostatic energy. In the present work a region 1 containing approximately 250 atoms was found to be sufficient to converge the absolute defect energy to approximately 0.01 eV, though relative energies will be far more converged than this.

The Schottky defects (i.e., $V_{\mathrm{Pb}}+2V_{\mathrm{F}}$) in the lattice are formed by moving the constituent ions to the surface from their bulk sites. On the other hand, the Frenkel defects are pairs of vacancies and interstitials of the same type of ion (i.e., $V_{\mathrm{Pb}}+\mathrm{Pb}_i$ and $V_{\mathrm{F}}+\mathrm{F}_i$). The formation energies of these defects given in Table IV were obtained from defect energy calculations of vacancies and interstitials in the lattice. As shown in this table, the lowest formation energy per defect comes out to be that for the Frenkel pair in the anion sublattice, which is followed by the Schottky trio and cation Frenkel pairs. We also include in Table IV the formation energy of di- and trivacancies, formed by the electrostatic aggregation of a Pb vacancy and one or two F vacancies. Their values indicate a strong tendency to create these aggregates, at least at room temperature.

TABLE IV. Formation energies (in eV) per defect in $\beta$-$PbF_2$.

| | | | |
|---|---|---|---|
| Frenkel | | Schottky | $E_S=1.96$ |
| F | $E_F=0.69$ | Divacancy | $E_D=-0.41$ |
| Pb | $E'_F=4.25$ | Trivacancy | $E_T=-0.74$ |

### B. Transport properties

The temperature dependence of the ionic conductivity, $\sigma_T$, is experimentally known to assume several Arrhenius-like steps,

$$\sigma_T = \sigma_0/T \exp\{-E^a/kT\}, \tag{3}$$

being $k$ Boltzmann's constant, in which the pseudoactivation energy $E^a$ can also be written as

$$E^a = -k\left(\frac{\partial \ln T\sigma_T}{\partial 1/T}\right). \tag{4}$$

In order to have a microscopic level interpretation, it is assumed that

$$\sigma_T = \sum_i x_i q_i \mu_i, \tag{5}$$

where $x_i$, $q_i$, and $\mu_i$ are the concentration, charge, and mobility of the different defects $i$. The $1/T$ Nernst-Einstein dependence in Eq. (3) comes from $\mu_i$; the exponential behavior can be attributed to similar exponential behaviors of $x_i$ and $\mu_i$, and the different steps correspond to changes in the dominant conducting species, owing to the overcoming of the different exponential terms in Eq. (5). Thus

$$E^a = -k\left(\frac{\partial \ln x_i}{\partial 1/T} + \frac{\partial \ln(T\mu_i)}{\partial 1/T}\right) = E_i^c + E_i^m \tag{6}$$

will be the pseudoactivation energy for the step dominated by $i$ species conductivity, that can be split into concentration ($E_i^c$) and mobility ($E_i^m$) dependent terms. The exponential behavior of the mobility is easily assigned to the activation energy barrier for ionic migration in defect $i$, a kinetic term. On the other hand, $E_i^c$ should be due to the equilibrium concentration of defect $i$, a thermodynamic effect, for which we are *assuming* the exponential dependency with temperature.

For each defect reaction $0 \Rightarrow \Sigma_i \nu_i A_i$ between species $A_i$ with signed stoichiometric coefficients $\nu_i$, we can write the mass-action law as $K = \Pi_i x_i^{\nu_i}$, where $K$ is the equilibrium constant. $K$ changes with temperature according to the van 't Hoff equation,

$$\Delta H = -k\left(\frac{\partial \ln K}{\partial 1/T}\right)_P. \tag{7}$$

Substituting the mass-action law, and remembering the definition of $E_i^c$, we find that

$$\Delta H = \sum_i \nu_i E_i^c. \tag{8}$$

Considering the reaction energies of several defect reactions and the external restrictions over the concentrations, we could solve a set of linear equations to find the different concentration contributions to the activation energies, $E_i^c$. In the case of $PbF_2$, we will include the anion ($0 \Rightarrow F_i + V_F$, $\Delta H = E_F$) and cation ($0 \Rightarrow Pb_i + V_{Pb}$, $\Delta H = E_F'$) Frenkel defect formation reactions, the Schottky defect formation ($0 \Rightarrow V_{Pb} + 2V_F$, $\Delta H = E_S$, where we have omitted the ions that go to the surface since they do not contribute to the mass-action law), and the aggregation energy for divacancies ($V_{Pb} + V_F \Rightarrow$ divacancy, $\Delta H = E_D$) and trivacancies ($V_{Pb} + 2V_F \Rightarrow$ trivacancy, $\Delta H = E_T$). We will take into account three different conditions: (i) $V_F$ excess due to extrinsic impurities, which will make $x_{V_F}$ constant and therefore $E^c_{V_F} \simeq 0$; (ii) intrinsic behavior (pure material), where fluorine Frenkel defects will dominate and then we could could make $x_{V_F} \simeq x_{F_i}$ and thus $E^c_{V_F} \simeq E^c_{F_i}$; and (iii) $F_i$ extrinsic excess, with $x_{F_i}$ constant and $E^c_{F_i} \simeq 0$. Solving the set of equations on each of these three conditions, we obtain the concentration contributions to the activation energies listed in Table V.

TABLE V. Concentration contributions to the activation energies for several defect species $i$, $E_i^c$, computed for different concentration conditions.

| Defect | (i) $V_F$ excess | (ii) Intrinsic regime | (iii) $F_i$ excess |
|---|---|---|---|
| $V_F$ | 0 | $E_F/2$ | $E_F$ |
| $F_i$ | $E_F$ | $E_F/2$ | 0 |
| $V_{Pb}$ | $E_S$ | $E_S - E_F$ | $E_S - 2E_F$ |
| $Pb_i$ | $E_F' - E_S$ | $E_F' - E_S + E_F$ | $E_F' - E_S + 2E_F$ |
| Divacancy | $E_D + E_S$ | $E_D + E_S - E_F/2$ | $E_D + E_S - E_F$ |
| Trivacancy | $E_T + E_S$ | $E_T + E_S$ | $E_T + E_S$ |

In order to compute the migration energies $E_i^m$, we will take them to be equivalent to the energy barrier for the migration, that is, the difference between the minimum energy for the defect and the energy saddle point along the migration path (maximum in the direction of the path, minimum in all other directions). We will consider the following migra-

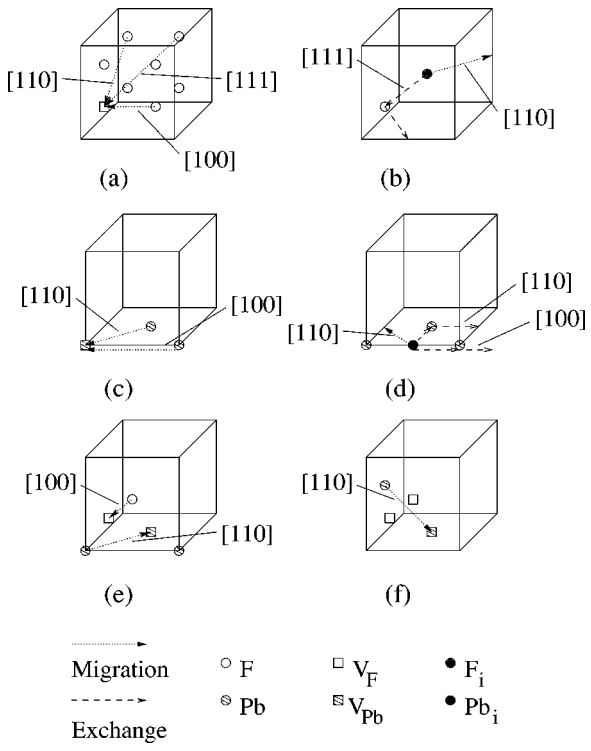


FIG. 2. Migration paths within the crystallographic $PbF_2$ unit cell: (a) $V_F$ migration; (b) $F_i$ migration and exchange; (c) $V_{Pb}$ migration; (d) $Pb_i$ migration and exchange; (e) $V_{Pb}$ and $V_F$ divacancy migration; (f) $V_{Pb}$ migration in a trivacancy.

TABLE VI. Migration ($E^m$) and concentration-corrected activation energies ($E^a$) for several ionic conductivity mechanisms with different concentration conditions: (i) $V_F$ excess; (ii) intrinsic regime; (iii) $F_i$ excess. All energies in eV.

| Mechanism | | $E_i^m$ | $E^a$(i) | $E^a$(ii) | $E^a$(iii) |
|---|---|---|---|---|---|
| $V_F$ | ⟨100⟩ | 0.29 | 0.29 | 0.64 | 0.98 |
| | ⟨110⟩ | 1.05 | 1.05 | 1.40 | 1.74 |
| | ⟨111⟩ | 0.98 | 0.98 | 1.33 | 1.67 |
| $F_i$ | ⟨110⟩ | 1.46 | 2.15 | 1.80 | 1.46 |
| | ⟨111⟩ exch. | 0.66 | 1.35 | 1.00 | 0.66 |
| $V_{Pb}$ | ⟨100⟩ | 2.77 | 4.74 | 4.05 | 3.36 |
| | ⟨110⟩ | 1.40 | 3.37 | 2.68 | 1.99 |
| $Pb_i$ | ⟨110⟩ | 2.31 | 4.60 | 5.28 | 5.98 |
| | ⟨100⟩ exch. | 1.34 | 3.63 | 4.32 | 5.01 |
| | ⟨110⟩ exch. | 1.25 | 3.53 | 4.22 | 4.91 |
| Divacancy | F migration | 0.25 | 1.80 | 1.45 | 1.11 |
| | Pb migration | 0.98 | 2.53 | 2.18 | 1.84 |
| Trivacancy | Pb migration | 1.50 | 2.72 | 2.72 | 2.72 |

TABLE VII. Formation energy of isolated rare-earth dopants ($E_M$), binding energies of the dopant-interstitial NN and NNN complexes, and the difference in NN and NNN binding energies ($\Delta$BE). All energies in eV, and the formation energy of an isolated $F_i$ is $-2.72$ eV.

| System | $E_M$ | BE(NN) | BE(NNN) | $\Delta$BE |
|---|---|---|---|---|
| $PbF_2:Y^{+3}$ | −24.23 | −0.67 | −0.44 | −0.23 |
| $PbF_2:La^{+3}$ | −20.43 | −0.76 | −1.07 | 0.31 |
| $PbF_2:Ce^{+3}$ | −22.16 | −0.37 | −0.55 | 0.18 |
| $PbF_2:Pr^{+3}$ | −22.78 | −0.34 | −0.44 | 0.10 |
| $PbF_2:Nd^{+3}$ | −22.86 | −0.21 | −0.42 | 0.21 |
| $PbF_2:Sm^{+3}$ | −23.08 | −0.22 | −0.45 | 0.23 |
| $PbF_2:Eu^{+3}$ | −23.19 | −0.42 | −0.54 | 0.12 |
| $PbF_2:Gd^{+3}$ | −23.29 | −0.38 | −0.53 | 0.15 |
| $PbF_2:Tb^{+3}$ | −23.49 | −0.23 | −0.50 | 0.27 |
| $PbF_2:Dy^{+3}$ | −23.62 | −0.24 | −0.63 | 0.39 |
| $PbF_2:Er^{+3}$ | −23.89 | −1.10 | −0.80 | −0.30 |
| $PbF_2:Yb^{+3}$ | −24.16 | −0.56 | −0.25 | −0.31 |
| $PbF_2:Lu^{+3}$ | −24.15 | −0.84 | −0.49 | −0.35 |

tion paths: $V_F$ migration along the ⟨100⟩, ⟨110⟩, and ⟨111⟩ directions [Fig. 2(a)], $F_i$ migration along ⟨110⟩ and exchange (concerted path only) along ⟨111⟩ [Fig. 2(b)], $V_{Pb}$ migration along ⟨100⟩ and ⟨110⟩ [Fig. 2(c)], $Pb_i$ migration along ⟨110⟩ and exchange along ⟨100⟩ and ⟨110⟩ [Fig. 2(d)], divacancy migration with $V_{Pb}$ along ⟨110⟩ or $V_F$ along ⟨100⟩ [Fig. 2(e)], and trivacancy $V_{Pb}$ ⟨110⟩ migration [Fig. 2(f)]. The resulting migration energies are listed in the second column of Table VI.

After adding the migration and concentration activation-like energies, we obtain the results listed in the last three columns of Table VI. It is interesting to note that the concentration change with temperature is dominant in ruling out some mechanisms. For instance, the F migration within a divacancy cluster has the smallest migration energy, but its concentration increases very slowly with temperature. Overall, $V_F$ and $F_i$ will be the preferred carriers for vacancy- and interstitial-rich samples at low temperature, whereas $V_F$ will be the preferred one for extremely pure samples or when temperature makes the intrinsic defect concentration important.

With respect to the cation migration, the preferred mechanism will be the $V_{Pb}-V_F$ divacancy one, owing to its low energy barrier. The traditionally assumed mechanism,[25] the ⟨110⟩ $V_{Pb}$ migration, is still the preferred one among the single-defect mechanisms, and even better than the trivacancy mechanism. For fluorine vacancy excess conditions, the trivacancy mechanism can compete with the divacancy and, for interstitial excess conditions, the single vacancy mechanism is also within the range of the divacancy mechanism.

We can now compare our results with the experimental data of Samara.[26] Accordingly, for low temperatures where the extrinsic concentration of defects dominates, $A$(alkali)F-doped $PbF_2$ exhibits a pseudo-activation energy $E^a$ of $0.26\pm0.02$ eV, while $M$(rare-earth)$F_3$-doped samples have an $E^a$ of $0.52\pm0.03$ eV. The first one is in excellent agreement with our vacancy-excess $E^a$ for the ⟨100⟩ $V_F$ conduction mechanism, 0.29 eV, whereas the second one corresponds to our interstitial-excess value for the ⟨111⟩ $F_i$ exchange mechanism. The somewhat higher value might be due to the concerted movement assumption (relaxing the coordinates of both $F^-$ ions would lead to a lower energy saddle), since the fluorine Frenkel defect energy is already very small. At higher temperatures, both vacancy and interstitial excess samples have a transition to a new regime with activation energy $0.73\pm0.02$ eV. This agrees with a transition to intrinsic defect conduction by means of fluorine vacancies, although our value, 0.64 eV, is smaller. This leads us to believe that calculations find a lower fluorine Frenkel defect $E_F$ value, although by a small amount. This is also consistent with the results for higher temperatures. Samara has found an activation energy of $1.03\pm0.03$ eV, whereas our result for the $F_i$ exchange mechanism is 1.00 eV. A lowering of this mechanism barrier by means of relaxation, accompanied by a twice as great increase of the Frenkel energy, would leave this activation energy as it is, while cor-

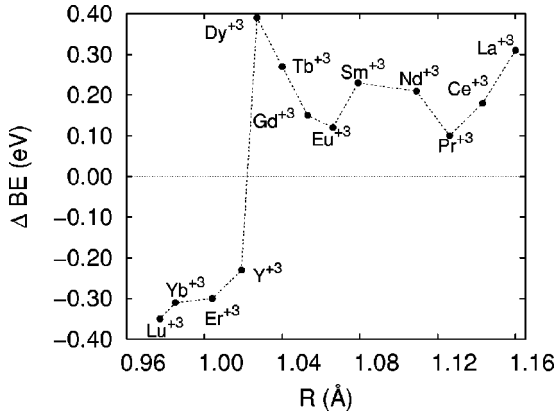


FIG. 3. Variation of the difference between binding energies of NN and NNN complexes with the dopant size. Positive values indicate NNN preference, negative values NN preference. The turnout occurs for ionic radii around 1.025 Å.

recting those of the previous stages. The overall agreement is good, and confirms the mechanism assignments proposed by Samara.

### C. Rare-earth doped $PbF_2$

Rare-earths in alkaline-earth fluorides are known to enhance the superionic conductivity of the host fluorides.[27] This enhancement appears to be linked to a tendency of rare earths to form aggregates of different sizes with intrinsic defects in the fluoride lattice. In alkaline-earth fluorides, defect aggregation has been thoroughly studied by Catlow and his co-workers,[15,28–31] with an aim to provide a microscopic description of the aggregation process. In the present case of $PbF_2$, aggregation of intrinsic defects has been observed[10] which also seems to play an important role in its conductivity.[32]

In this section, we now present our results for the formation of discrete cluster complexes containing a trivalent dopant-ion substituting $Pb^{+2}$ and a fluorine interstitial ($F_i$) which compensates the excess charge due to the dopant in the lattice. The cluster complexes in the cubic $PbF_2$ lattice, can generally be formed in two ways, namely nearest neighbor (NN) and next nearest neighbor (NNN). In the NN complex, dopant and $F_i$ are nearest neighbors [i.e., dopant at (0,0,0) and $F_i$ at (1/2,0,0)] while dopant and $F_i$ are next-nearest neighbors [i.e., dopant at (0,0,0) and $F_i$ at (1/2,1/2,1/2)] in the lattice. The substitutional dopant has therefore a tetragonal and trigonal symmetry in the NN and NNN complexes, respectively.

It is well known[28] that the ratio of tetragonal to trigonal defects is very sensitive to the lattice parameter of the host (alkaline-earth fluoride) crystal. We can also expect, by analogy with divalent dopants in alkali halides[33] and the previous work of Catlow and co-workers in similar crystals,[15] that the substitutional preference is strongly dependent on the size of a dopant-ion.

In Table VII we present the computed association energies for the formation of the two types of dopant-interstitial pairs in the $PbF_2$ crystal for various rare-earth ($M^{+3}$) ions. We also list the difference between the binding energies of the NN and NNN complexes. Accordingly, rare-earth dopants are predicted to be stable in both NN and NNN complexes. However, a clear preference for the NNN complex is seen with the increase in the size of the dopant in the lattice. This fact is further evident from Fig. 3 where the difference in binding energies is plotted against the dopant-size given by the Shannon ionic radii.[34]

The variation of binding energies of either NN or NNN cluster complexes can be explained simply in electrostatic terms. The dominant contribution to the binding energy of such complex is due to the Coulombic interaction between dopant and $F_i$. This interaction term varies with the inverse of the distance, so that small $M^{+3}$ ions prefer $F_i$ as nearest neighbors to minimize the separation of the charged defects, and thus electrostatically stabilize the complex. When the dopant-size is larger, short-range repulsive interactions between the shared fluorine ions and dopant (or $F_i$) overcome the Coulombic interaction, leading to the stability of the NNN complex over the NN complex.

Our results can also be compared with a similar study on rare-earth doped $CaF_2$, $SrF_2$, and $BaF_2$.[28] Overall, the calculated binding energies in $PbF_2$ fall perfectly within the trends shown by rare earths in the alkaline-earth fluoride family. The NN complex is predicted to be the preferred one for a crystal with a small lattice parameter in this fluoride family. This is indeed the case in $CaF_2$ where the NN complex is relatively more stable for all $M^{+3}$ cations. On the other hand, $F_i$ in $BaF_2$ is predicted to prefer the NNN site for all $M^{+3}$ cations. The calculated results on rare-earth doped $SrF_2$ are, however, intermediate between the results on $CaF_2$ and $BaF_2$, having some NN and some NNN complexes as the most stable ones in the lattice. The results on $PbF_2$ are therefore expected to be similar to those of $SrF_2$, since the lattice parameters (in bohr) are reported to be 10.3232, 10.9303, 11.6917, and 11.2126 for $CaF_2$, $SrF_2$, $BaF_2$, and $PbF_2$, respectively.[35] This similarity is also reflected in the Shannon ionic radii for cubic coordination, 1.26, 1.42, and 1.29 Å for $Sr^{+2}$, $Ba^{+2}$, and $Pb^{+2}$, respectively.[34] The predicted behavior of the (dopant-$F_i$) binding energy in $PbF_2$ is therefore justified in terms of the predicted stability of the NN complex for a fluoride lattice with a small lattice parameter.

## IV. SUMMARY AND CONCLUSIONS

We have obtained another set of shell-model parameters for $PbF_2$ which reproduce its bulk properties very well. Due to the high polarizability of the $Pb^{+2}$ cation, a quartic term in the core-shell interaction is required for a convergence of calculations involving defects. The Frenkel defect-pair of fluorine is predicted to be the most stable defect and is likely to dominate the defect chemistry of $\beta$-$PbF_2$. We have also considered the ionic conductivity in terms of mobility and concentration effects, obtaining a good agreement with the available experimental results. Finally, we have derived interatomic potential parameters representing interactions of the host-lattice ions with rare-earth dopants, and have studied the stability of dopant-fluorine interstitial cluster complexes. It is found that the dopant size is determinant in the preferred position of the fluorine interstitial in $PbF_2$.

## ACKNOWLEDGMENTS

J.D.G. acknowledges the Royal Society for financial support. M.A.B. thanks the Spanish Ministerio de Educación for funding his stay at MTU. This work was partially supported by DGICyT grant PB96-0559.

*Permanent address: Departamento de Química Física y Anlítica, Universidad de Oviedo, 33006-Oviedo, Spain.

†Permanent Address: Departamento de Química Física y Analítica, Universidad de Oviedo, 33006-Oviedo, Spain. Corresponding author: mblanco@mtu.edu

‡Permanent Address: Department of Physics, Tongji University, Shanghai 200092, China.

[1] F. Nessi-Tedadi, Nucl. Instrum. Methods Phys. Res. A **408**, 266 (1998).

[2] A. Lempicki and A. J. Wojtowicz, J. Lumin. **60&61**, 942 (1994).

[3] P. Lecoq, J. Lumin. **60&61**, 948 (1994).
[4] S. E. Derenzo, W. W. Moses, J. L. Cahoon, R. C. C. Perera, and J. E. Litton, IEEE Trans. Nucl. Sci. **37**, 203 (1990).
[5] G. A. Samara, Phys. Rev. B **13**, 4529 (1976).
[6] J. Oberschmidt and D. Lazarus, Phys. Rev. B **21**, 2952 (1980).
[7] D. Z. Shen, G. H. Ren, Q. Deng, and Z. W. Yin, Sci. Sin. **28**, 46 (1998).
[8] G. H. Ren, Ph.D. thesis, Shanghai Institute of Ceramics, 1998.
[9] S. F. Matar, C. R. A. Catlow, and J. M. Réau, Solid State Ionics **9&10**, 511 (1983).
[10] S. F. Matar, J. M. Réau, P. Hagenmuller, and C. R. A. Catlow, J. Phys. Chem. Solids **45**, 453 (1984).
[11] C. R. A. Catlow and W. C. Mackrodt, in *Computer Simulation of Solids*, edited by C. R. A. Catlow and W. C. Mackrodt, Lecture Notes in Physics (Springer, New York, 1982).
[12] M. P. Tosi, Solid State Phys. **16**, 1 (1964).
[13] B. J. Dick and A. W. Overhauser, Phys. Rev. **112**, 90 (1958).
[14] J. D. Gale, J. Chem. Soc., Faraday Trans. **93**, 629 (1997).
[15] C. R. A. Catlow, A. V. Chadwick, and J. Corish, J. Solid State Chem. **48**, 65 (1983).
[16] J. D. Gale, Philos. Mag. B **73**, 3 (1996).
[17] G. Simmons and H. Warg, *Single Crystal Elastic Constants and Calculated Aggregated Properties: A Handbook*, 2nd ed. (MIT Press, Boston, MA, 1971).
[18] *Handbook of Physics Properties of Rocks III*, edited by R. S. Carmichael (CRC Press, Boca Raton, FL, 1982).
[19] *Crystal Data; Determinative Tables*, 3rd ed., edited by H. M. Ondik and G. M. Wolter (US National Bureau of Standards, Washington D.C., 1972), Vol. 2.
[20] E. Francisco, J. M. Recio, M. A. Blanco, A. M. Pendás, and L. Pueyo, Phys. Rev. B **51**, 2703 (1995).
[21] T. Koga, S. Watanabe, K. Kanayama, R. Yasuda, and A. J. Thakkar, J. Chem. Phys. **103**, 3000 (1995).
[22] T. Koga, K. Kanayama, S. Watanabe, T. Imai, and A. J. Thakkar (unpublished).
[23] H. Lee, C. Lee, and R. G. Parr, Phys. Rev. A **44**, 768 (1991).
[24] E. Clementi, S. J. Chakravorty, G. Corongiu, and V. Sonnad, in *Modern Techniques in Computational Chemistry: MOTECC-90*, edited by E. Clementi (ESCOM Science Publishers, Leiden, 1990), Chap. 2, pp. 47–140.
[25] C. R. A. Catlow, M. J. Norgett, and T. A. Ross, J. Phys. C **10**, 1627 (1977).
[26] G. A. Samara, J. Phys. Chem. Solids **40**, 509 (1979).
[27] C. R. A. Catlow, J. D. Comins, F. A. Germano, R. T. Harley, W. Hayes, and I. B. Owen, J. Phys. C **14**, 329 (1981).
[28] J. Corish, C. R. A. Catlow, P. W. M. Jacobs, and S. H. Ong, Phys. Rev. B **25**, 6425 (1982).
[29] P. J. Bendall, C. R. A. Catlow, J. Corish, and P. W. M. Jacobs, J. Solid State Chem. **51**, 159 (1984).
[30] C. R. A. Catlow, A. V. Chadwick, J. Corish, L. M. Moroney, and A. N. O'Reilly, Phys. Rev. B **39**, 1897 (1989).
[31] D. Bingham, A. N. Cormack, and C. R. A. Catlow, J. Phys.: Condens. Matter **1**, 1213 (1989).
[32] A. Rhandour, J. M. Réau, S. F. Matar, and P. Hagenmuller, J. Phys. Chem. Solids **47**, 587 (1986).
[33] J. Corish, J. M. Quigley, P. W. M. Jacobs, and C. R. A. Catlow, Philos. Mag. A **44**, 13 (1981).
[34] R. D. Shannon, Acta Crystallogr., Sect. A: Cryst. Phys., Diffr., Theor. Gen. Crystallogr. **32**, 751 (1976).
[35] R. W. G. Wyckoff, *Crystal Structures* (Interscience Publishers, Inc., New York, 1960), Vol. II.